Experimental electronic structure of Be_2C

C.-T. Tzeng
Institute of Electro-Optical Engineering, National Chiao-Tung University, Hsinchu, Taiwan, Republic of China

K.-D. Tsuei
Synchrotron Radiation Research Center, Hsinchu, Taiwan, Republic of China
and Department of Physics, National Tsing-Hua University, Hsinchu, Taiwan, Republic of China

W.-S. Lo
Synchrotron Radiation Research Center, Hsinchu, Taiwan, Republic of China
(Received 12 March 1998)

The insulating Be_2C thin films have been successfully prepared on a Be surface. A low-energy electron diffraction pattern shows that the films have (100) orientation along the surface normal. We have used angle-resolved photoemission to map out the occupied bulk band dispersion along the Γ-X direction. The band-gap edges at the X point are 6.7 and 11.5 eV below the valence-band maximum, which is located at the Γ point. These values are in good agreement with theoretical calculations. The unoccupied bulk electronic structure is measured using C 1s near-edge x-ray-absorption spectroscopy. The spectrum is similar in shape to the energy-loss spectrum and the calculated p-partial density of states, while the peak positions are different. [S0163-1829(98)01335-6]

I. INTRODUCTION

The insulating crystal, beryllium carbide (Be_2C) is believed to be a strongly ionic crystal. Its strong chemical bonding leads to high melting temperature, which implies potential use as refractories and large elastic constants, which, in turn, are related to hardness, high sound velocities and good thermal conductivity. It has been found that Be_2C is even harder than silicon carbide.[1,2] It is also found that beryllium carbide is highly resistant to radiation damage and may be used as a component of fission reactor fuels and as a blanket material for fusion reactors.[3,4] The possible large band gap ($\sim$3 eV), though not exactly determined, might lead to interesting optical properties and other potential technological applications.

There are few theoretical calculations investigating the structural and electronic properties of Be_2C.[5–7] The general conclusion is that it is strongly ionic with an indirect band gap (Γ-X) larger than 1.2 eV. On the experimental side, to our knowledge, there is only one paper reporting the electronic structure by using a high-energy electron microscope combined with electron energy-loss spectroscopy (EELS) in the low-energy-loss region, as well as Be and C 1s near-edge fine structures.[8] The scarcity of experimental electronic studies is due to the nature of the Be_2C samples. Preparation of Be_2C is difficult because it is a high-temperature ceramic that easily hydrolyzes to $Be(OH)_2$ and reacts with O and N. In the EELS study the sample was a fine powder with a high concentration of BeO. The largest crystals found were about 1 μm in diameter and these were usually surrounded by BeO-rich particles. This sample size is not suitable for optical absorption and photoemission experiments, in which macroscopic beams of mm size are typically used, to obtain spectra entirely from Be_2C crystals.

We report in this paper a way to prepare Be_2C single-crystal films large enough for macroscopic studies. The occupied valence-band structure is mapped by angle-resolved photoemission. The result is in good agreement with recent calculations. The unoccupied conduction band density of states is measured by C 1s near-edge photoabsorption. The Be and C 1s core-level binding energies measured by photoemission are found to be consistent with the description of strongly ionic bonding of the compound.

II. EXPERIMENT

Be_2C has the fcc antifluorite structure, which is the same as the calcium fluorite structure, but with the anion and cation interchanged. The C atoms occupy fcc sites and each C atom is surrounded by eight Be atoms at $(\pm 1/4, \pm 1/4, \pm 1/4)a$, where $a = 4.342$ Å is the lattice constant.[9] The structure is similar to the diamond structure but with all tetrahedral sites filled by Be. Not only the structure but also electronically this compound is isovalent to the group-IV elemental semiconductors and III-V semiconductor compounds.

The experiment was carried out at the Synchrotron Radiation Research Center in Hsinchu, Taiwan using LSGM and HSGM beamlines. The photoemission was carried out in an ultrahigh-vacuum (UHV) chamber equipped with low-energy electron diffraction (LEED) and a 200-mm radius hemispherical analyzer aligned with a fixed 50° angle to the incident photon beam. The base pressure was 1×10^{-10} torr. For angle-resolved valence-band photoemission the angular acceptance was $\pm1°$. Photon energies from 18 to 115 eV were used, and the spot size was less than 2 mm. The overall energy resolution was 0.1 eV at 20 eV, 0.15 eV at 80 eV, and 0.2 eV at 110 eV. For core-level photoemission an acceptance angle of $\pm8°$ was used, and photon energies of 150 eV for a Be 1s core and 320 eV for a C 1s core to maximize the intensity. The overall energy resolution was 0.2 and 0.4 eV for Be 1s and C 1s, respectively. For the C 1s near-edge x-ray-absorption fine structure (NEXAFS) measurement total electron yield detection was used and the

signal was normalized to the photocurrent from a freshly evaporated Au mesh placed in front of the sample. The incident angle was 50° to the surface normal. The photon energy was calibrated by photoemission from the second-order light. It was also checked by monitoring the mesh current in front of the sample and comparing the characteristic absorption dips due to carbon contamination of the beamline.

III. RESULTS AND DISCUSSION

A. Sample preparation, core-level photoemission, and LEED study

The sample was prepared by evaporating a thick layer of C_{60} onto a clean Be(0001) surface at room temperature. The Be crystal of $5\times10\ mm^2$ size was cleaned by cycles of Ar ion sputtering and annealing. The evaporation procedure has been described previously.[10] This C_{60} on Be(0001) surface was then annealed successively and monitored by core-level photoemission until no change in core-level binding energies can be detected. This final annealing temperature is 450 °C. Detailed C_{60} reaction on Be(0001) surface and Be_2C film growth will be presented elsewhere.[11] The Be_2C film thickness was not exactly known. It can be estimated that one monolayer of close-packed C_{60} with the same density as bulk (fcc) (111) plane density (with nearest-neighbor distance 10.02 Å) can result in a thickness of 14 Å Be_2C or 3.25 conventional unit cells along the [100] direction. This represents a lower limit of film thickness. Further depositions of C_{60} were used to increase the Be_2C film thickness that we believe was more than several tens of angstroms. The strong valence-band dispersion to be discussed later indicates that the film is thick enough to present the bulk electronic structure. The (100) surface can have either Be or C termination. The exact termination is not known and awaits further study. However, it does not affect the measured bulk band structure.

The C 1*s* core-level photoemission spectrum from Be_2C is shown in Fig. 1(a). For comparison the core-level photoemission from a 2 monolayer (ML) C_{60} film is shown in Fig. 1(b). It can be seen that the binding energy of C_{60} is 284.5 eV with respect to the substrate Fermi level, while for Be_2C the binding energy decreases by 2 eV to become 282.5 eV.[12] The Be 1*s* core-level photoemission spectrum from Be_2C is displayed in Fig. 2(a). For comparison the core-level photoemission from a clean Be(0001) surface is displayed in Fig. 2(b). The sharp clean surface peak at 111.2 eV and the shoulder at about 111.8 eV are due to unresolved surface and bulk peaks as discussed in the literature.[13] For Be_2C the Be 1*s* binding energy increases to 112.75 eV. This increase in Be core binding energy and decrease in C core binding energy are consistent with large charge transfer from Be to C as discussed previously.[5,6] Furthermore, we observe that the core-level peaks of Be_2C are wider than C_{60} and clean Be core-level peaks, and are slightly asymmetric. This may be due to inhomogeneity of the film or surface effect.

The LEED pattern from this prepared surface is schematically drawn in Fig. 3(a). Weak twelvefold spots could only be seen around 144 eV kinetic energy. We analyze the pattern as three domains of (100) surface as depicted by the three large squares rotated by 120°. The azimuthally elongated shape of spots indicates that the direction of each domain is only approximately aligned. These spots are then due to (20) and (02) diffraction. The deduced lattice constant is in perfect agreement with that of Be_2C fcc crystal. Spots likely corresponding to the (10), (01), and (11) diffraction at lower kinetic energies are very faint and difficult to see. The reason is not understood. The weak LEED spots imply that the surface consists of domains of [100] direction with the size comparable to, but not much larger than, the coherent

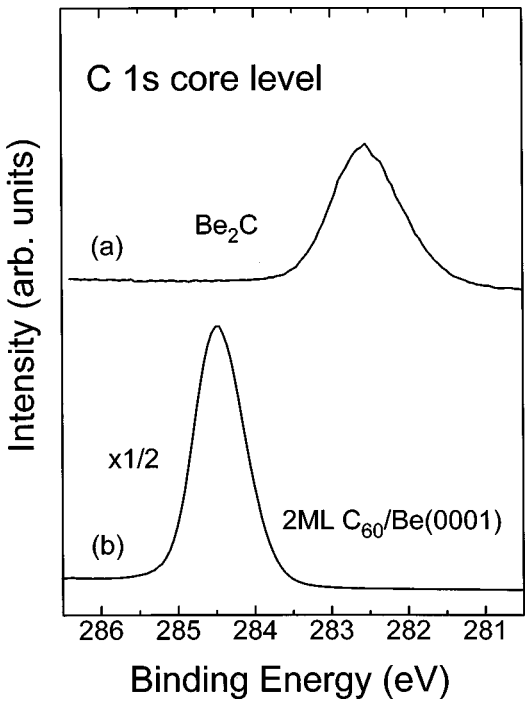

FIG. 1. C 1*s* core-level photoemission spectra from (a) Be_2C, and (b) 2 ML C_{60} film on a Be(0001) surface.

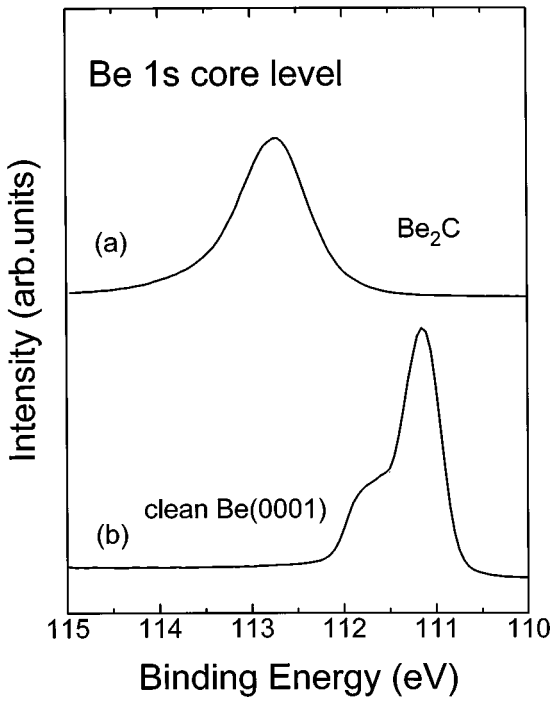

FIG. 2. Be 1*s* core-level photoemission spectra from (a) Be_2C, and (b) clean Be(0001) surface.

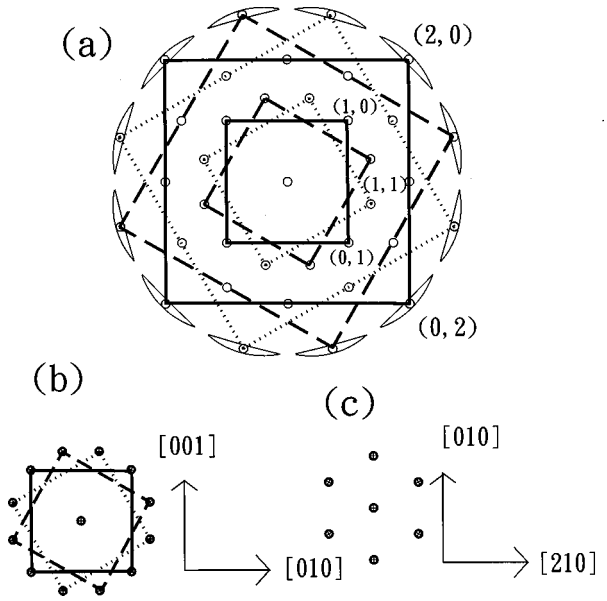

FIG. 3. (a) Schematic LEED pattern from the Be_2C film at 114 eV electron energy. The twelvefold new-moon shaped spots are observed and identified as due to (20) and (02) spots of three domains of (100) surface rotated by 120°. The open circles are representations of (10), (01), and (11) spots. (b) The corresponding real-space conventional cells of each domain and the symmetry direction of the domain marked by a solid square. (c) A real-space conventional cell of the Be(0001) substrate underlying the Be_2C film and the symmetry direction.

length of LEED, that is of the order of 100 Å. For clarity we add in Fig. 3(a) the presumed (10) and (01) spots, denoted as small open circles and connected by the three small squares, and the presumed (11) spots, in addition to the observed (20) and (02) spots. Figure 3(b) shows the corresponding real-space conventional cells of each domain and the symmetry direction of the domain marked by a solid square. Figure 3(c) shows a real-space conventional cell of the Be(0001) substrate underlying the Be_2C film. It can be seen that the twelve diffraction spots are in line with the substrate hexagonal structure, and the three domains of $Be_2C(100)$ surface are confined by the substrate threefold symmetry.[14] This seems reasonable because twice the nearest-neighbor distance of Be(0001) along the [010] direction, or twice the Be lattice constant a, is only 5% larger than the Be_2C lattice constant, and the nearest-neighbor distance of Be along the [210] direction is 9% less than the Be_2C lattice constant. The twelve spots can be equally well explained as due to the (11) diffraction from four domains of $Be_2C(111)$ surface. However, the substrate surface does not have fourfold symmetry and the valence-band dispersion is consistent with the [100], not with the [111], direction as explained in the next subsection.

B. Valence-band mapping by angle-resolved photoemission

In direct transition of photoemission the conservation of energy and momentum leads to

$$E_f(\mathbf{k}_f) = E_i(\mathbf{k}_i) + h\nu, \tag{1}$$

where E_i and E_f are the initial- and final-state energies, $\mathbf{k}_i = \mathbf{k}$ is the electron's initial momentum in the reduced zone scheme, $\mathbf{k}_f = \mathbf{k} + \mathbf{G}$ is final momentum and $\mathbf{G}$ is the bulk reciprocal lattice vector, and $h\nu$ is the photon energy. Since we focus here on photoemission along the direction normal to the surface, both the initial and final momenta, $\mathbf{k}$ and $\mathbf{k} + \mathbf{G}$, can be assumed along the surface normal in most cases. It has been found that the high-lying final states can well be described by a free electronlike dispersion,[15]

$$E_f(\mathbf{k}_f) = \hbar^2 |\mathbf{k}_f|^2/2m + E_0, \tag{2}$$

where $|\mathbf{k}_f| = k_\perp$ for normal emission, and E_0 is the ''bottom of the muffin tin'' referenced to the valence-band maximum (VBM) and is to be determined experimentally. Once E_0 is known the final state $k_\perp$ can be calculated in the extended-zone scheme as

$$\hbar k_\perp = [2m(E_i + h\nu - E_0)]^{1/2}, \tag{3}$$

and the initial state $k_\perp$ in the reduced-zone scheme is

$$(k_\perp)_{\text{red}} = k_\perp - G \tag{4}$$

with an appropriate G.

Although the Be_2C thin film consists of many domains with the azimuthal directions not well aligned one can still measure the band dispersion using angle-resolved normal emission as long as the [100] axis is along the surface normal. This is exactly what we observed here. Figure 4 displays a series of photoemission spectra at various photon energies at the normal emission geometry. The binding energy is referenced with respect to the substrate Fermi energy. We first discuss the dispersive peaks. Below 50 eV [Fig. 4(a)] the prominent peak labeled $P15$ disperses to the critical point of Γ_{15} at a photon energy of 22 eV, which gives the valence-band maximum (VBM) at 1.32 eV. We note here that there is no emission at the Fermi energy; therefore, this film is insulating with a band gap of at least 1.32 eV. This peak disperses down in energy and diminishes in intensity between 52 and 68 eV photon energies as shown in Fig. 4(b). Another peak at 7.5 eV shows up at 52 eV photon energy and becomes the most prominent peak at 68 eV photon energy with a binding energy of 8.0 eV and labeled $P1$, where the critical point X_4' is reached. Starting at 68 eV photon energy another bulk transition disperses to a maximum of 12.8 eV at 72 eV photon energy (X_1) and then disperses downwards as shown in Fig. 4(c) and labeled $B1$. In Fig. 4(a) there is another dispersive peak labeled $B2$ in a photon energy range of 28–46 eV. Its origin will be discussed later.

Figure 5 summarizes the peak binding energies found in Fig. 4 as a function of photon energy. In this figure the bulk transitions are represented by solid and open circles. The extreme positions of the dispersive peaks mark the Brillouin-zone center and boundary and can be used to determine an experimental value of E_0. For example, the extreme position of $P15$ at the VBM for $h\nu = 22$ eV corresponds to the transition at the zone center to a final $k_\perp = 2(2\pi/a) = 2\Gamma X = G_{200}$. Using Eq. (3) we obtain the experimental value of $E_0 = -9.7$ eV. Similarly, $P1$ at 68 eV and $B1$ at 72 eV correspond to the transition at the zone boundary of the X point with a final $k_\perp = (3/2)G_{200}$. The obtained E_0 values are quite similar. This indicates that our analysis using a free-electron final band is valid. We note here that E_0 lies just inside the band gap at X and L points, similar to the case of GaAs.[15] For clarity we plot in Fig. 5 the dispersion curves as

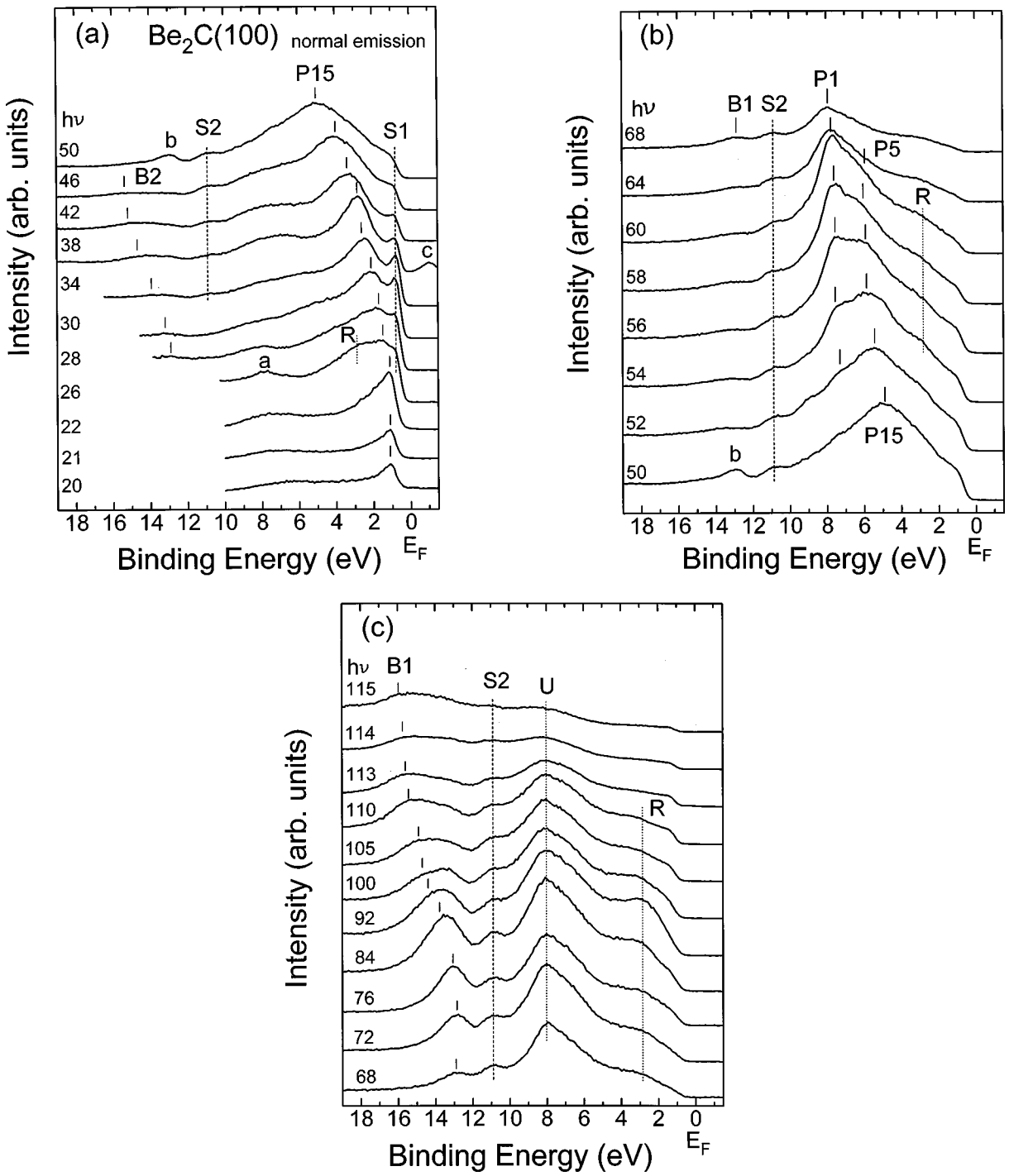

FIG. 4. Angle-resolved photoemission spectra collected at the normal emission geometry for the photon energy range, (a) 20–50 eV, (b) 50–68 eV, and (c) 68–115 eV. The intensities are normalized to sample currents and rescaled in each panel. Peak *c* in (a) at 38 eV photon energy is the Be 1*s* core level excited by the fourth-order radiation. The binding energy is referenced to the substrate Fermi energy.

the solid lines using the theoretical initial-state bands along the [100] direction (Γ-X) calculated by Corkill and Cohen,[6] and our experimentally determined final-state free-electron-like bands. The peaks $P15$, $P1$, and $P5$ between 22 and 68 eV photon energies are transitions to a final band of $k + G_{200}$. The peak $B1$ is mainly due to transitions to $k + G_{-400}$.

There are several nondispersive peaks. Peak $S1$ at 0.8 eV is above the VBM in the fundamental gap and $S2$ at 10.8 eV is in the gap between X_1 and X_4'; therefore they are ascribed as surface states. Their other properties will be discussed elsewhere.[11] At photon energies higher than 68 eV there is a peak U showing no dispersion with a binding energy exactly the same as the X_4' point (6.7 eV with respect to the VBM). This can be understood as due to secondary cone-surface umklapp emission.[15–17] Bloch final states that consist mainly of Fourier components moving in the directions other than the surface normal ($\mathbf{k}_f \nparallel \mathbf{n}$) may have a component moving along the surface normal, $[(\mathbf{k}_f + \mathbf{G}') \parallel \mathbf{n}]$ thus can be detected. An alternative interpretation is surface umklapp pro-

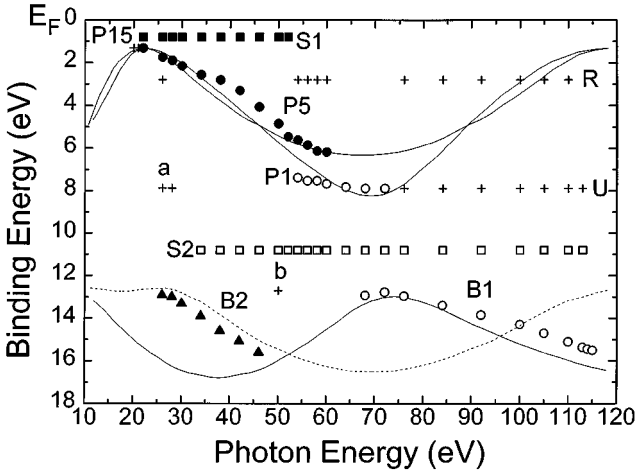

FIG. 5. Peak binding energies at various photon energies, shown as circles, crosses, squares, and triangles, deduced from Fig. 4. The solid line is the expected dispersion based on direct transition from the calculated initial bands along [100] from Ref. 6 to the experimentally determined final-state free-electron bands. The dashed line is the simulated dispersion along [110].

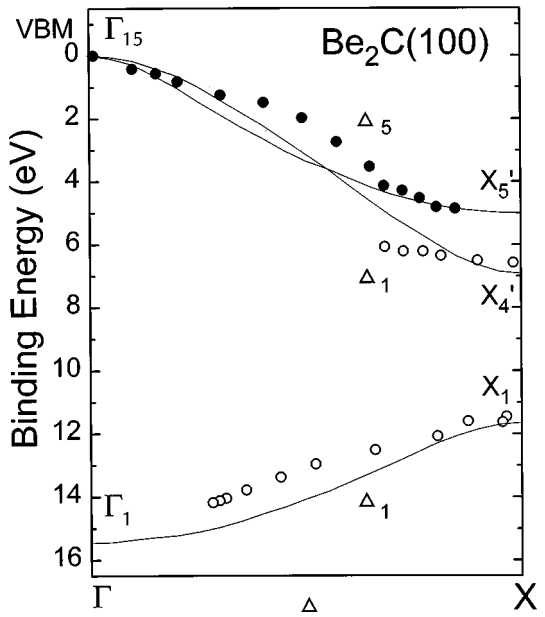

FIG. 6. Comparison of experimental initial band dispersion, shown as filled and open circles, with theoretical calculation, shown as curved lines, from Ref. 6 along Γ-X [100] direction. The binding energy is referenced to the VBM.

cess in that the final state is still the plane-wave state ($\mathbf{k}_f$) moving along an off-normal direction while it is scattered back to the normal direction by a surface reciprocal lattice vector $\mathbf{G}_s$, which exactly cancels the parallel component of the final state. The relation between these two reciprocal space vectors is simply $\mathbf{G}_s = \mathbf{G}'_{\parallel}$. Due to lifetime broadening the contributing states are smeared out forming more or less a continuum in the E versus k space. Therefore, these processes result in nondispersive peaks in the spectra that reflect valence-band one-dimensional critical points with high density of states along the surface normal. In our case peak U at 68 eV photon energy coincides with $P1$ at critical point X'_4. It is composed of an ordinary transition to $k+G_{200}$ and $k+G_{-400}$, where $k=(2\pi/a)(1,0,0)$, as well as an off-normal transition to $k+G_{-2\pm2\pm2}$ and $k+G_{0\pm2\pm2}$. Peak U at 107 eV corresponds to off-normal transitions to $k+G_{2\pm20}$, $k+G_{20\pm2}$, $k+G_{-4\pm20}$, and $k+G_{-40\pm2}$. There are also peaks at binding energies the same as critical points while appearing only in the small photon energy range. This appears at relatively low photon energy because the lifetime broadening is smaller and the available transitions are less. Peak b of 12.9 eV binding energy at 50 eV photon energy corresponds to transitions from X_1 to $k+G_{1\pm1\pm1}$, and $k+G_{-3\pm1\pm1}$, and fits into this category. The peak a at around 26 eV photon energy has a binding energy exactly the same as X'_4. However, we could not explain it using the above model.

The nondispersive peak labeled R deserves a special discussion. It is revealed as a feature in three photon energy ranges of 28–30 eV, 54–60 eV, and 72–110 eV. Its binding energy does not correspond to any critical point energy at Γ or X points, therefore it cannot be explained by the above models. On the other hand, its binding energy to the VBM, 1.5 eV, is close to the calculated L'_3 point of 2 eV.[6] Nevertheless it seems difficult to comprehend how one can observe a direct transition from the L point in normal emission from a (100) surface. Even if we do have (111) domains, as would be consistent with LEED, the corresponding final-state bands are not consistent with the direct transition model. However, an electron from a transition from the L point may be detected in normal emission from a (100) surface if the surface provides a reciprocal-space lattice vector $G_s/2$, where G_s $[=(2\pi/a)(0,\pm1,\pm1)]$ is the reciprocal-space unit vector of the fcc(100) surface, which assists the surface umklapp process. Evidence of this possibility is that the photon energies needed for transitions from the L point $[k=(2\pi/a)(1/2,1/2,1/2)]$ to $k+G_{0-2-2}$, $k+G_{02-2}$, and $k+G_{022}$ final states are 28, 60, and 92 eV, respectively, and these energies correspond well to the observation. Transition to these three final bands has relatively larger probability than to other bands because of their relatively larger ratio of $|k_{\parallel}/k_{\perp}|$, and thus longer time in the surface region.[17] The reciprocal-space lattice vector $G_s/2$ can exist if the surface undergoes a (2×1) or (2×2) reconstruction although we did not observe it in the very weak LEED pattern.

The dispersive $B2$ peak between 28 and 46 eV, marked by filled triangles in Fig. 5, is also difficult to understand. Its dispersion range is similar to $B1$ but $B2$ cannot be explained by any of the above models. In Fig. 5 we plot with a dashed line the band dispersion using the theoretical initial-state bands along [110] direction (Γ-K-X) and our experimentally determined final-state bands. The agreement with $B2$ dispersion is reasonably good. This is a puzzling result since we have no evidence of (110) surface. An explanation could be that the film might contain domains of (110) surface. These domains must be small because we do not see (110) LEED pattern and their fraction must also be small because the corresponding $B2$ intensity is extremely weak. Photoemission from such small (110) domains could be detected only when the intensity from the major (100) domains vanish due to low cross sections.

The usual dispersion relation E-versus-k is shown in Fig. 6 for ΓX (Δ). The initial-state binding energy referenced to the VBM is used here. The experimental data are presented

TABLE I. Critical point energies [with respect to the VBM (Γ_{15})] and band gaps by experiment and theories for Be_2C (in eV).

	APW[a]	PPPW[b]	FP[c]	Expt.
Critical points				
Γ_1	−14.0	−15.5	−15.2	
X_1	−10.8	−11.6	−11.5	−11.5
X_4'	−5.6	−7.0	−6.9	−6.7
X_5'	−3.9	−5.1	−5.0	
L_2'	−7.1	−9.2	−9.0	
L_3'	−1.5	−2.0	−2.0	
Band gaps				
X_1-X_4'	5.2	4.6	4.6	4.8
Γ_{15}-X_1	3.0	1.24	1.21	>1.3

[a]Augmented plane-wave calculation (Ref. 5).
[b]Pseudopotential plane-wave calculation (Ref. 6).
[c]Full potential calculation (Ref. 7).

as filled and open circles. The theoretical dispersion curves, shown as solid lines, are from Ref. 6. It can be seen that the calculation agrees well to the measurement. In Table I we compare the measured critical point energies with the available calculations. Other calculations yield very similar results and the agreement with our measurement is also good.

C. NEXAFS

The C 1*s* NEXAFS of Be_2C is shown in Fig. 7 as filled circles. The EELS data by Disko *et al.* is also shown as open circles for comparison.[8] The NEXAFS peak at 284.5 eV appears in EELS as a small shoulder. The double peak group around 288 eV in NEXAFS is lower by 1 eV than EELS peak near 289 eV. The sharp peak at 292.7 eV and a shoulder at 295 eV in NEXAFS correspond to a relatively flat structure in EELS. The discrepancy might be due to different detection schemes. The onset of absorption in our data is at 282.5 eV, which may represent the conduction-band minimum (CBM). Since the C 1*s* core-level and the VBM binding energies (with respect to the substrate Fermi level) are 282.5 and 1.3 eV, respectively, we may deduce the fundamental band gap (Γ_{15}-X_1) as 1.3 eV. However, the local unoccupied state energy is expected to shift down in the presence of a core hole in NEXAFS process. This correction is unknown. Therefore, the value 1.3 eV can only be viewed as a lower bound of the band gap measured by other methods, and is consistent with the result from valence-band photoemission as discussed earlier. The calculated *p*-partial density of states (*p*-PDOS) broadened by a 2.5 eV width Gaussian function at the C site by Lee, Lambrecht, and Segall is also displayed as a dashed line for comparison.[7] Since no absolute energy reference with respect to core level exists in the calculation, we plot the *p*-PDOS curve according to the authors to align the major peaks with EELS data. That is equivalent to setting the calculated VBM at 282.5 eV and the CBM at 283.7 eV. This is apparently inconsistent with our data, thus indicating a likely shift or scaling between calculation and measurement. From the comparison between the calculated low-energy-loss function, which involves valence and conduction bands, with the measurement by Disko *et al.*,[8] Lee, Lambrecht, and Segall found that a rigid shift of 2 eV would result in good agreement and the latter estimated that the fundamental gap would be about 3 eV. The calculated PDOS and band structure may provide us with information of where the absorption peaks come from.[5,7] The NEXAFS double-peak group around 288 eV can be from the lowest conduction band in the region of the Brillouin zone near the *L* point, where the bands are quite flat. (See Fig. 1 of Ref. 7.) The peak at 284.5 eV in NEXAFS is from the lowest conduction band slightly higher than the *X* point (CBM). A shoulder also appears in the calculated PDOS in Ref. 5 while it does not show up in Ref. 7; this feature is probably washed out by the large broadening of 2.5 eV used in the latter calculation.

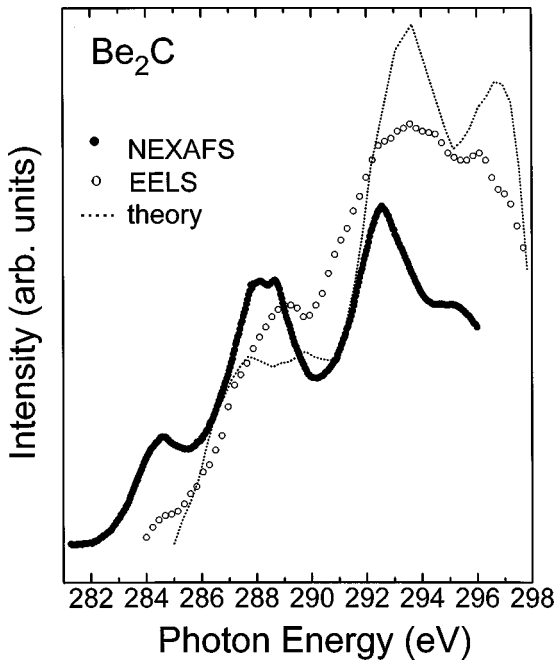

FIG. 7. Comparison of our NEXAFS data, shown as filled circles, EELS data, shown as open circles, from Ref. 8, and calculated *p*-PDOS, shown as dotted lines, from Ref. 7.

IV. CONCLUSION

We have found a way to produce single-crystal Be_2C films for measurements with macroscopic (mm) beam size. The major part of the occupied valence-band structure measured by angle-resolved photoemission agrees well with recent calculations. The unoccupied conduction band PDOS was measured by C 1*s* NEXAFS and is in reasonably good agreement with the EELS result and calculated *p*-PDOS, while the peak positions are different.

ACKNOWLEDGMENTS

We thank the staff of the SRRC for providing technical support, especially J.-Y. Yuh and R.-Y. Chu for assisting with the taking of data. One of us (K.D.T.) is thankful to J.-L. Chen for providing results of all his electron LDA calculations and for useful discussions, and to E. W. Plummer for the loan of a Be crystal. This work was supported in part by the National Science Council of the Republic of China.

[1] J. H. Coobs and W. J. Koshuba, J. Electrochem. Soc. **99**, 115 (1952); M. W. Malett *et al.*, *ibid.* **101**, 298 (1952).
[2] L. H. Rovner and G. R. Hopkins, Nucl. Technol. **29**, 274 (1976).
[3] E. P. Roth, Int. J. Thermophys. **3**, 45 (1982).
[4] H. Migge, J. Nucl. Mater. **103**, 687 (1981).
[5] P. Herzig and J. Redinger, J. Chem. Phys. **82**, 372 (1984).
[6] J. L. Corkill and M. L. Cohen, Phys. Rev. B **48**, 17 138 (1993).
[7] C. H. Lee, W. R. L. Lambrecht, and B. Segall, Phys. Rev. B **51**, 10 392 (1995).
[8] M. M. Disko, J. C. H. Spence, O. F. Sankey, and D. Saldin, Phys. Rev. B **33**, 5642 (1986).
[9] R. W. G. Wyckoff, *Crystal Structures*, 2nd ed. (Interscience, New York, 1963), Vol. 1, p. 241.
[10] K.-D. Tsuei, J.-Y. Yuh, C.-T. Tzeng, R.-Y. Chu, S.-C. Chung, and K.-L. Tsang, Phys. Rev. B **56**, 15 412 (1997).
[11] C.-T. Tzeng, K.-D. Tsuei, W.-S. Lo, J.-Y. Yuh, and R.-Y. Chu (unpublished); the key points to successfully prepare clean Be_2C films from reaction of C_{60} films on Be surfaces are the low evaporation temperature of C_{60} (450 °C), low annealing temperature, and UHV environment; the former two conditions cannot be achieved using the other two forms of carbon, graphite, and diamond.
[12] The C 1*s* binding energy relative to the Fermi energy of graphite, which is metallic, is also 284.5 eV, the same as thick C_{60} films, which is insulating, on metal substrates. See T. Gouder, C. A. Colmenares, and J. R. Naegele, Surf. Sci. **342**, 299 (1995), and Ref. 10.
[13] L. I. Johanson, H. I. P. Johanson, J. N. Andersen, E. Lungren, and R. Nyholm, Phys. Rev. Lett. **71**, 2453 (1993).
[14] The clean substrate LEED pattern shows, on the other hand, sixfold spots due to its hcp structure and stepped surface.
[15] T.-C. Chiang, J. A. Knapp, M. Aono, and D. E. Eastman, Phys. Rev. B **21**, 3513 (1980).
[16] G. D. Mahan, Phys. Rev. B **2**, 4334 (1970).
[17] B. S. Itchkawitz, I.-W. Lyo, and E. W. Plummer, Phys. Rev. B **41**, 8075 (1990).